Structural Engineering and Mechanics, *Vol. 66, No. 3 (2018) 411-421*
DOI: https://doi.org/10.12989/sem.2018.66.3.411

Dynamic response of a base-isolated CRLSS with baffle

Xuansheng Cheng*[1], Bo Liu[1], Liangliang Cao[1], Dongpo Yu[2] and Huan Feng[2]

[1]*Key Laboratory of Disaster Prevention and Mitigation in Civil Engineering of Gansu Province, Lanzhou University of Technology, Lanzhou, 730050, PR China*
[2]*Western Engineering Research Center of Disaster Mitigation in Civil Engineering of Ministry of Education, Lanzhou University of Technology, Lanzhou, 730050, PR China*

(Received September 19, 2016, Revised May 3, 2018, Accepted May 4, 2018)

Abstract. Although a rubber isolation cushion can reduce the dynamic response of a structure itself, it has little influence on the height of a sloshing wave and even may induce magnification action. Vertical baffles are set into a base-isolated Concrete Rectangular Liquid Storage Structure (CRLSS), and baffles are opened as holes to increase the energy dissipation of the damping. Problems of liquid nonlinear motion caused by baffles are described using the Navier-Stokes equation, and the space model of CRLSS is established considering the Fluid-Solid Interaction (FSI) based on the Finite Element Method (FEM). The dynamic response of an isolated CRLSS with various baffles under an earthquake is analyzed, and the results are compared. The results show that when the baffle number is certain, the greater the number of holes in baffles, the worse the damping effects; when a single baffle with holes is set in juxtaposition and double baffles with holes are formed, although some of the dynamic response will slightly increase, the wallboard strain and the height of the sloshing wave evidently decrease. A configuration with fewer holes in the baffles and a greater number of baffles is more helpful to prevent the occurrence of two failure modes: wallboard leakage and excessive sloshing height.

Keywords: isolation; concrete; rectangular liquid storage structure; baffle; liquid-solid interaction; dynamic response

1. Introduction

With the rapid development of the world economy and the daily increase in world population escalating daily, the pace of urbanization construction is accelerating, and various industries are rapidly developing. Because of their low cost, simple structure and convenient availability of the materials, concrete liquid storage structures, regarded as important strategic reserve structures, are widely used in various modern industrial fields, particularly in larger water storage equipment (for example, waterworks and sewage treatment plants); at the same time, they can also be used for large oil storage (including flammable, explosive, toxic, stimulating and volatile liquid) structures in petrochemical enterprises. CRLSSs are used in national lifeline engineering. However, concrete is a material with a very complex constitutive relationship, and the research of CRLSS is still in a state of relative lag in the seismic aspect. In July 1952, an earthquake with Ms 7.7 struck California in the USA. Researchers have found that most supports at the bottom of the storage tank were damaged, and explosion and fire then occurred. In July 1976, many cracks were formed in an oil tank wall in the Tangshan earthquake. The earthquake caused serious damage to the oil tank, reducing its bearing capacity, so a large amount of radioactive liquid spilled. All of these events had an inestimable influence on the ecological environment surrounding life.

At present, researchers have been highly focused on the liquid sloshing of liquid storage structures. In recent years, the use of large liquid storage equipment has increased in the petrochemical enterprises. Thus, many scholars have had a strong interest in FSI of liquid-storage structures, and they have systematically studied the encountered problems (Virella *et al.* 2008, Zhao *et al.* 2006, Chen 2008, Bao 2003, Li *et al.* 2011) in practical applications. Wilson (2002) proposed the concept of FSI vibration in a report on dam water pressure under earthquakes. Kianoush and Ghaemmaghami (2011) investigated the effect of earthquake frequency content on the seismic behavior of fluid rectangular tank system by four different seismic motions. Nayak and Biswal (2013) analyzed nonlinear seismic response of rectangular liquid tank. The model was presented by Cakir and Livaoglu (2011) by using Housner's two-mass approximation for fluid interaction and mass-spring-dashpot system for backfill interaction. Panchal *et al.* (Panchal and Soni 2014, Goudarzi and Alimohammadi 2010, Jadhav and Jangid 2006) studied seismic response of base-isolated liquid storage tanks. Liu *et al.* (2010) ran a simulation of waves caused by shaking in three-dimensional fluid using the SPH method and summed up the movement characteristic of three-dimensional fluid. Sui *et al.* (2011) established a simulation model of a liquid storage structure under the effect of an external excitation seismic load, successfully simulating the shock effect of liquid in a tank acting on a wallboard under an earthquake; they also analyzed the amplitude of liquid sloshing under an earthquake and presented some measures to reduce it. Jia *et al.* (2012) analyzed the model and dynamic response on the liquid-solid problems of a liquid storage structure by using the finite element software program ANSYS and

*Corresponding author, Professor
E-mail: chengxuansheng@gmail.com

ISSN: 1225-4568 (Print), 1598-6217 (Online)

summarized the sloshing law. Cheng *et al.* (2015a, b, c) studied the dynamic response of base-isolated CRLSS without baffles. Vosoughifar and Naderi (2014) used the finite element method to investigate the seismic behavior of rectangular liquid tanks in three-dimensional domains. The continuous liquid mass of the tank was modeled as lumped masses referred as convective mass, impulsive and rigid mass. Eswaran *et al.* (2015) studied the slosh height and the possibility of water spill from rectangular Spent Fuel Storage Bays (SFSB) and Tray Loading Bays (TLB) of Nuclear power plant (NPP) during 0.2 g, safe shut down earthquake (SSE) level of earthquake.

At present, certain achievements in the isolation of liquid storage structures have been obtained by researchers. Although conventional rubber isolation can reduce the dynamic response of a liquid storage structure itself, it is not good for the damping effect of liquid sloshing. Thus, in this paper, by arranging baffles inside the base-isolated CRLSS, on the one hand, the isolation can reduce the structural seismic response; one the other hand, the baffle can make up for the inefficient of the isolation for reducing the sloshing height of liquid. Through establishing a corresponding calculation model considering FSI, the dynamic responses of stress, strain, displacement and range of liquid surface fluctuation regarding the base-isolated CRLSS with various baffles under an earthquake are studied. Thus, the issue that needs attention in the baffle design of a base-isolated CRLSS is discussed.

2. Solution of FSI

2.1 Governing equation of liquid domain

The fluid control equation for liquid storage structures is

$$\nabla^2 p = 0 \tag{1}$$

FEM is used to solve the above equation based on existing boundary conditions.

2.2 Boundary condition of free liquid

Considering the slight shaking of the free surface, the boundary condition is

$$\frac{1}{g}\frac{\partial^2 p}{\partial t^2} + \frac{\partial p}{\partial z} = 0 \tag{2}$$

where z is the vertical direction, and g is the gravitational acceleration.

2.3 Boundary condition of liquid-wallboard interface

On the interface between liquid and a wallboard, liquid does not flow in the direction of the vertical wallboard, and the boundary must meet the condition

$$\frac{\partial p}{\partial n} = -\rho a_n^s \tag{3}$$

where n is the normal direction of the wallboard, and the a_n^s is the acceleration acting on liquid in the n direction.

2.4 Discrete equation of fluid domain

With the Galerkin method, the finite element discrete equation of the fluid domain can be expressed as (Mirzabozorg *et al.* 2012)

$$\mathbf{G}\ddot{\mathbf{P}} + \mathbf{C_f}\dot{\mathbf{P}} + \mathbf{K_f}\mathbf{P} = \mathbf{F} \tag{4}$$

In Eq. (4), each item can be expressed as

$$G_{ij}^e = \frac{1}{g}\int_{A_e} N_i N_j dA;$$

$$H_{ij}^e \int_{V_e}\left(\frac{\partial N_i}{\partial x}\frac{\partial N_j}{\partial x} + \frac{\partial N_i}{\partial y}\frac{\partial N_j}{\partial y} + \frac{\partial N_i}{\partial z}\frac{\partial N_j}{\partial z}\right)dV;$$

$$\mathbf{F} = \mathbf{F_i} - \rho\mathbf{Q}^{\mathrm{T}}\left(\ddot{\mathbf{U}} + \ddot{\mathbf{U}}_{\mathbf{g}}\right);\quad F_i^e = \int_{A_e} N_i \frac{\partial p}{\partial n} dA.$$

where **P** is liquid pressure matrix, N_i is shape function of node i of the liquid cell, $\ddot{\mathbf{U}}$ is the acceleration of the structure node, $\ddot{\mathbf{U}}_{\mathrm{g}}$ is the ground acceleration, $\mathbf{Q}$ is the interaction matrix, $\mathbf{G}$, $\mathbf{C_f}$ and $\mathbf{K_f}$ are the mass, damping and stiffness matrices of the fluid domain, $\mathbf{F}$ is load matrix acting on the liquid domain.

2.5 Interaction matrix

The liquid pressure of the FSI interface can be passed to the wallboard by the interaction matrix $\boldsymbol{Q}$ in the form of nodal force. This matrix can be obtained by using the proportion agglomerate method. For an 8-node element that has translation degrees of freedom in the x, y and z directions and a 4-node element for which every node has a pressure degree of freedom, the interaction matrix can be expressed as (Mirzabozorg *et al.* 2012)

$$\boldsymbol{Q} = \omega\int_{-1}^{1}\int_{-1}^{1}\begin{bmatrix} \alpha_1 N_1^s N_1^s N_1^f & \cdots & \alpha_1 N_1^s N_1^s N_4^f \\ \beta_1 N_1^s N_1^s N_1^f & \cdots & \beta_1 N_1^s N_1^s N_4^f \\ \gamma_1 N_1^s N_1^s N_1^f & \cdots & \gamma_1 N_1^s N_1^s N_4^f \\ \vdots & \vdots & \vdots \\ \alpha_8 N_8^s N_8^s N_1^f & \cdots & \alpha_8 N_8^s N_8^s N_4^f \\ \beta_8 N_8^s N_8^s N_1^f & \cdots & \alpha_8 N_8^s N_8^s N_4^f \\ \gamma_8 N_8^s N_8^s N_1^f & \cdots & \gamma_8 N_8^s N_8^s N_4^f \end{bmatrix}_{24\times 4} \left\|\boldsymbol{t}_\xi \times \boldsymbol{t}_\eta\right\| d\xi d\eta \tag{5}$$

where each symbol can be expressed as

$$\boldsymbol{t}_\xi = \left\{\frac{\partial x}{\partial \xi}, \frac{\partial y}{\partial \xi}, \frac{\partial z}{\partial \xi}\right\}^T \quad ; \quad \boldsymbol{t}_\eta = \left\{\frac{\partial x}{\partial \eta}, \frac{\partial y}{\partial \eta}, \frac{\partial z}{\partial \eta}\right\}^T \quad ;$$

$$\omega = \frac{A}{\sum_{i=1}^{8}\int_{A_e} N_i^s N_i^s \left|t_\xi \times t_\eta\right| d\xi d\eta}; A = \int_{A_e}\left\|t_\xi \times t_\eta\right\| d\xi d\eta$$

where N^f is the shape function of the fluid domain, and N^s is the shape function of the structural domain, A_e is area of the

element, α_1, β_1, α_s and β_s are the direction cosines of the nodes of the surface element on the wet face of the structure.

2.6 Damping matrix of fluid region

The damping matrix of the fluid domain consists of two parts: an advection part and a pulse part (Mirzabozorg *et al.* 2012); it can be expressed as

$$\mathbf{C_f} = a\mathbf{G} + b\mathbf{K_f} \tag{6}$$

where a and b can be obtained by Rayleigh damping. a can be obtained based on the sloshing frequency of the free surface, and b can be obtained by using the fundamental frequency of the structure wallboard.

2.7 Structure control equation

$$\mathbf{M}_s\ddot{\mathbf{u}}_s + \mathbf{C}_s\dot{\mathbf{u}}_s + \mathbf{K}_s\mathbf{u}_s = -\mathbf{M}_s\ddot{\mathbf{u}}_g + \mathbf{P} \tag{7}$$

where $\mathbf{u}_s$, $\dot{\mathbf{u}}_s$ and $\ddot{\mathbf{u}}_s$ are the displacement, velocity and acceleration of the structure under the action of earthquake, respectively, $\ddot{\mathbf{u}}_g$ is the seismic acceleration, $\mathbf{P}$ is the liquid pressure, and $\mathbf{M}_s$, $\mathbf{C}_s$ and $\mathbf{K}_s$ are the mass matrix, stiffness matrix and damping matrix of the structure, respectively.

$$\mathbf{M}_s = \sum\int_V \mathbf{B}^T\mathbf{D}\mathbf{B}dV \quad , \quad \mathbf{K}_s = \sum\int_V \mathbf{N}^T\rho_s\mathbf{N}dV \quad ,$$

$$\mathbf{C}_s = \alpha\mathbf{M}_s + \beta\mathbf{K}_s, \quad \alpha = 2\frac{\omega_i\omega_j}{\omega_i+\omega_j}\xi_s, \quad \beta = \frac{2}{\omega_i+\omega_j}\xi_s$$

where, $\mathbf{B}$ is the strain matrix, $\mathbf{D}$ is the elastic matrix, $\mathbf{N}$ is the shape function matrix, ρ_s is the material density of the structure, α and β are the mass and stiffness damping coefficients, respectively, ξ_s is the structural damping ratio and is taken as 0.05, and ω_i and ω_j are the i- and j-order circular frequencies of the structure, respectively.

In this paper, Newmark-β method is adopted to solve the matrix differential equation, namely,

$$\mathbf{u}_{s,t+\Delta t} = \mathbf{u}_{s,t} + \Delta t\dot{\mathbf{u}}_{s,t} + \left(\frac{1}{2}-\varsigma\right)\Delta t^2\ddot{\mathbf{u}}_{s,t} + \varsigma\Delta t^2\ddot{\mathbf{u}}_{s,t+\Delta t} \tag{8}$$

$$\dot{\boldsymbol{u}}_{s,t+\Delta t} = \dot{\boldsymbol{u}}_{s,t} + (1-\tau)\Delta t\ddot{\boldsymbol{u}}_{s,t} + \tau\Delta t\ddot{\boldsymbol{u}}_{s,t+\Delta t} \tag{9}$$

where τ and ς are constants.

The motion differential equation at time t+Δt is

$$\mathbf{M}_s\ddot{\mathbf{u}}_{s,t+\Delta t} + \mathbf{C}_s\dot{\mathbf{u}}_{s,t+\Delta t} + \mathbf{K}_s\mathbf{u}_{s,t+\Delta t} = -\mathbf{M}_s\ddot{\mathbf{u}}_{g(t+\Delta t)} + \mathbf{P} \tag{10}$$

With regards to the basic parameters of Newmark-β, it is absolutely stable to choose $\tau = 0.5$, $\varsigma = 0.25$ and $\Delta t \le \frac{T_{max}}{100}$ (T_{max} is the maximum natural vibration period), and the result reaches the required accuracy.

Substituting Eqs. (8) and (9) into Eq. (10) results in

$$\left(\mathbf{M}_s + \frac{\Delta t}{2}\mathbf{C}_s\right)\ddot{\mathbf{u}}_{s,t+\Delta t} + \mathbf{C}_s\left(\dot{\mathbf{u}}_{s,t} + \frac{\Delta t}{2}\ddot{\mathbf{u}}_{s,t}\right) + \mathbf{K}_s\mathbf{u}_{s,t+\Delta t} = -\mathbf{M}_s\ddot{\mathbf{u}}_{g(t+\Delta t)} + \mathbf{P} \tag{11}$$

Table 1 Mooney-Rivlin material constants (N/m^2)

C1	C2	C3	C4	C5	C6
206000.0	1858.0	4100.0	100.0	0.0	28.1

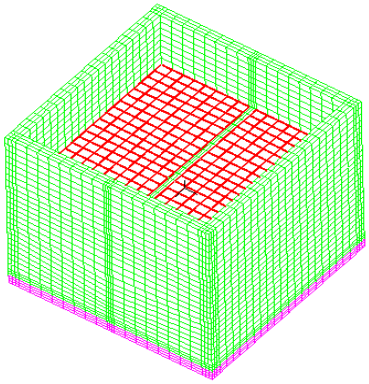

Fig. 1 Calculation model of isolated CRLSS

From Eq. (9), the following is obtained

$$\ddot{\mathbf{u}}_{s,t+\Delta t} = \frac{4}{\Delta t^2}\left(\mathbf{u}_{s,t+\Delta t} - \mathbf{u}_{s,t}\right) - \frac{4}{\Delta t}\dot{\mathbf{u}}_{s,t} - \ddot{\mathbf{u}}_{s,t} \tag{12}$$

Substituting Eq. (12) into Eq. (11) produces

$$\left(\mathbf{K}_s + \frac{2}{\Delta t}\mathbf{C}_s + \frac{4}{\Delta t^2}\mathbf{M}_s\right)\mathbf{u}_{s,t+\Delta t} = \mathbf{C}_s\left(\frac{2}{\Delta t}\mathbf{u}_{s,t} + \dot{\mathbf{u}}_{s,t}\right) + \mathbf{M}_s\left(\frac{4}{\Delta t^2}\mathbf{u}_{s,t} + \frac{4}{\Delta t}\dot{\mathbf{u}}_{s,t} + \ddot{\mathbf{u}}_{s,t}\right) - \mathbf{M}_s\ddot{\mathbf{u}}_{g(t+\Delta t)} + \mathbf{P} \tag{13}$$

$\mathbf{u}_{s,t+\Delta t}$ can be obtained from Eq. (13). $\ddot{\mathbf{u}}_{s,t+\Delta t}$ and $\dot{\mathbf{u}}_{s,t+\Delta t}$ can be obtained from Eq. (12) and Eq. (9), respectively.

3. Material parameters

A rubber cushion is used by the isolated system of CRLSS, and the constitutive model of the material is based on the hyper-elastic constitutive model (Bouabidi *et al.* 2013, Mirzabozorg *et al.* 2012) that is described by a strain energy density function and obtained by Mooney-Rivlin. The strain energy density function W that is described by the invariant of the deformation tensor is

$$W = \sum_{i+j-1}^{n} C_{ij}\left(I_i - 3\right)^i\left(I_j - 3\right)^j \tag{14}$$

where C_{ij} is a material constant, which is generally determined by experiment; I is the deformation tensor invariant; and the material constant is determined based on tension test of laminated rubber supports according to the literature. The Mooney–Rivlin material constants are shown in Table 1.

The thickness of the vibration isolation cushion of the model is chosen as 0.3 m. The model of whole rubber supports is built according to 3D solid element. The model is shown in Fig. 1.

The material parameters of the concrete, steel and fluid for the CRLSS model are shown in Table 2. The constitutive model, which considers the multi-axial and

Table 2 Material parameters

Material parameters	Steel	Concrete	Water
Elasticity modulus	2.0×10^{11} Pa	3×10^{10} Pa	—
Density	7800 kg/m^3	2500 kg/m^3	1000 kg/m^3
Poisson ratio	0.3	0.2	—
Initial yield strength	3.0×10^{8} Pa	—	—
Maximum equivalent plastic strain	0.0375	—	—
Modulus of strain hardening	1.0×10^{9} Pa	—	—
Shear modulus	2.0×10^{11} Pa	3.0×10^{10} Pa	—
Uniaxial tension test	—	2.01×10^{6} Pa	—
Tensile failure strength	—	1.5×10^{6} Pa	—
Uniaxial compressive strength	—	2.01×10^{7} Pa	—
Uniaxial compressive strain	—	-0.0018	—
Maximum uniaxial compressive strength	—	-1.0×10^{7} Pa	—
Maximum uniaxial compressive strain	—	-0.0033	—
Bulk modulus	—	—	2.3×10^{7} Pa

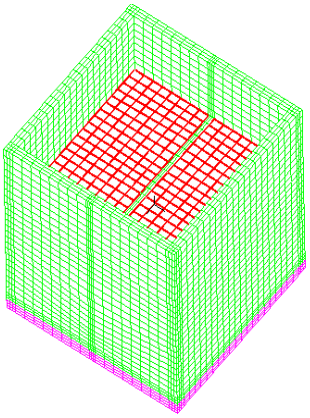

(a) Wallboard

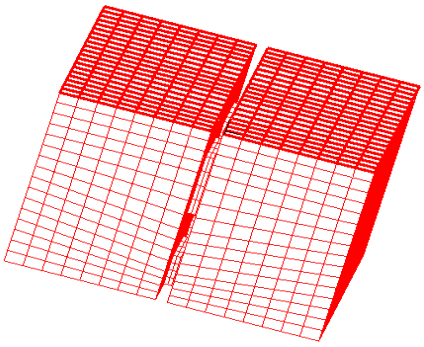

(b) Fluid

Fig. 2 Case of 1 baffle with 4 holes

shear, tension and compression effects, is used for the concrete material, and the constitutive model of bilinear elastic-plastic material is used for the steel, but the constitutive model used for the fluid is based on potential fluid.

4. Analysis model

The three-dimensional entity model of the isolated

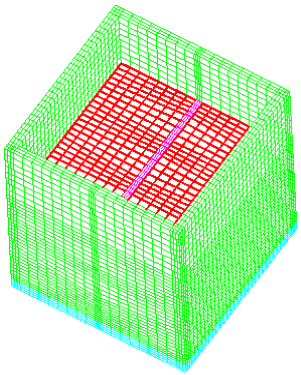

(a) Wallboard

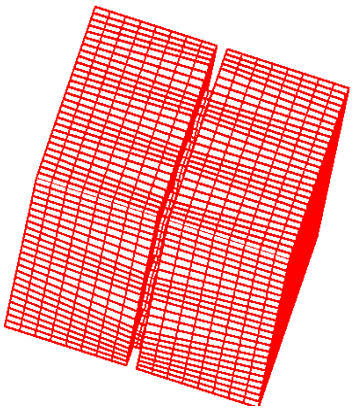

(b) Fluid

Fig. 3 Case of 1 baffle with 9 holes

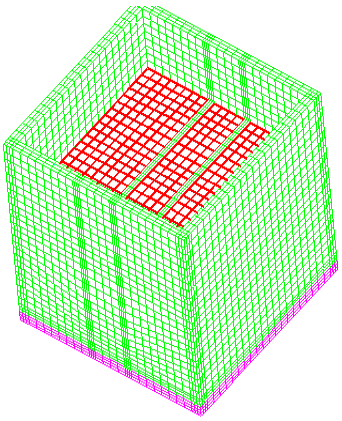

(a) Wallboard

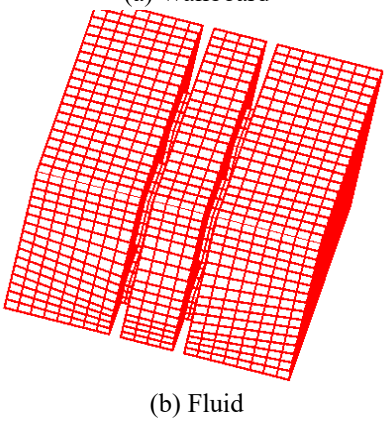

(b) Fluid

Fig. 4 Case of 2 baffles with 8 holes

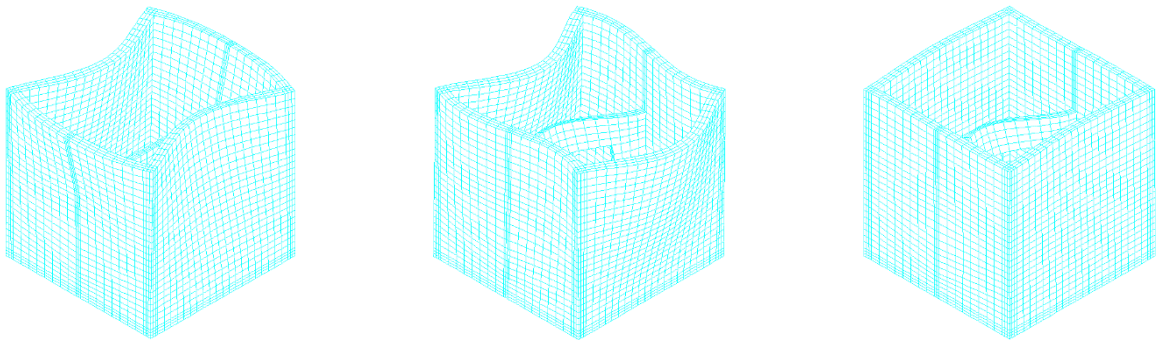

(f_1=25.34) (f_2=25.67) (f_3=27.16)

(a) Empty CRLSS without isolator

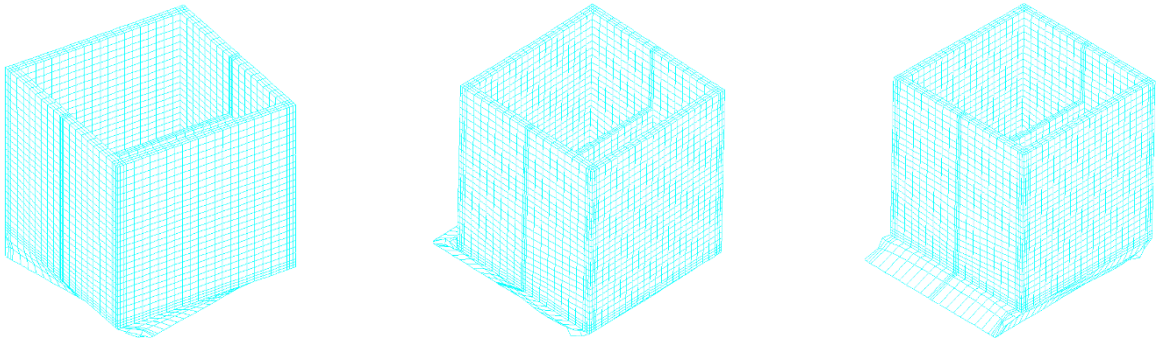

(f_1=2.442) (f_2=2.964) (f_3=2.980)

(b) Empty CRLSS with isolator

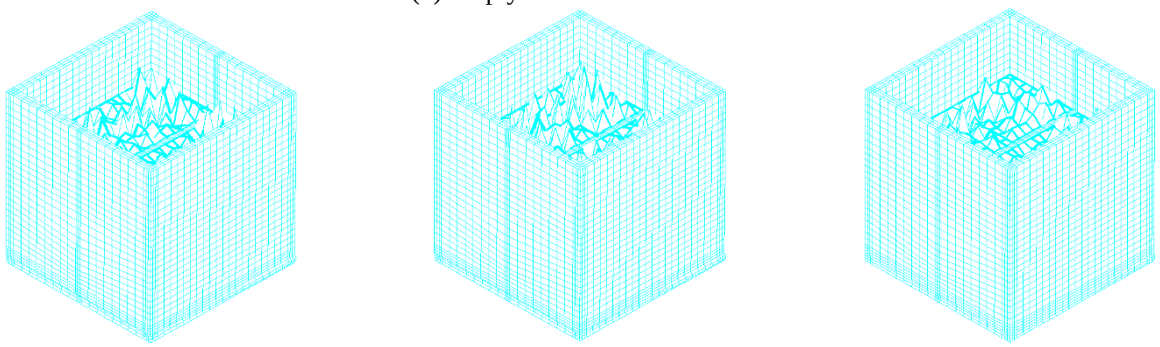

(f_1=0.3074) (f_2=0.4012) (f_3=2.980)

(c) Liquid filled CRLSS with isolator

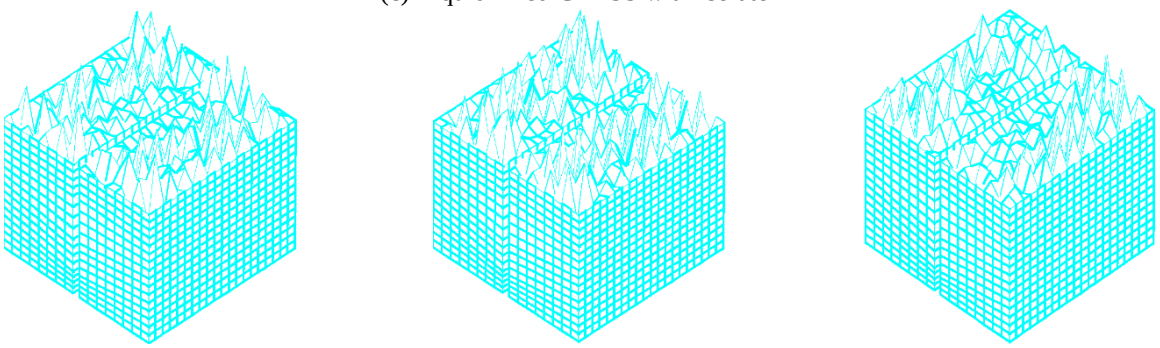

(f_1=0.3074) (f_2=0.4012) (f_3=2.980)

(d) Liquid

Fig. 5 First three mode shape and frequencies corresponding to 1 baffle with 4 holes

CRLSS with baffles (1 baffle with 4 holes, 1 baffle with 9 holes, and 2 baffles with 8 holes) is built. The length, width, and height of the CRLSS model are all 6 m, and the thicknesses of the surrounding plate and soleplate are all 0.3 m. A rubber isolation layer is installed at the bottom of CRLSS, and its thickness is 0.3 m. Mooney-Rivlin material model and 3-D Solid element are used to simulate the isolation layer. The fixed constraint is imposed at the

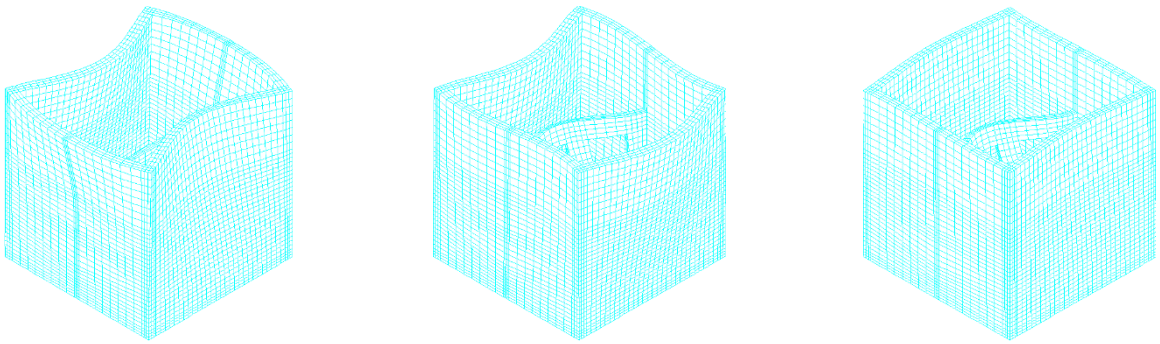

(f_1=25.14) (f_2=25.53) (f_3=26.58)

(a) Empty CRLSS without isolator

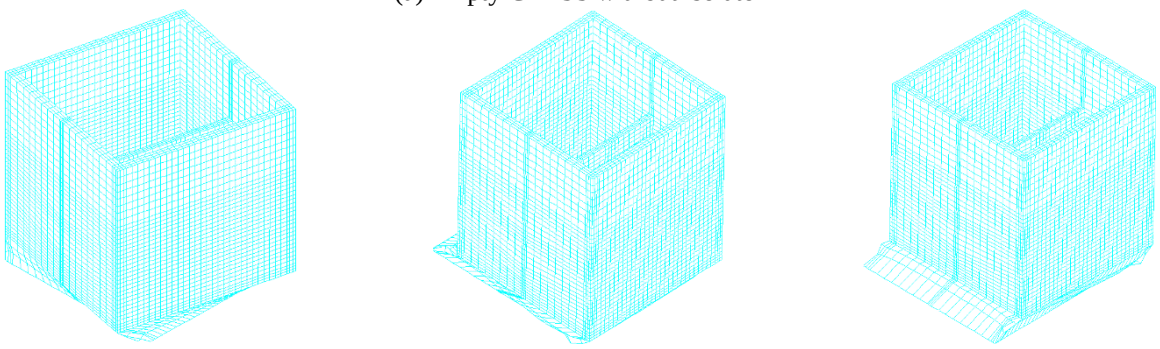

(f_1=2.444) (f_2=2.973) (f_3=2.987)

(b) Empty CRLSS with isolator

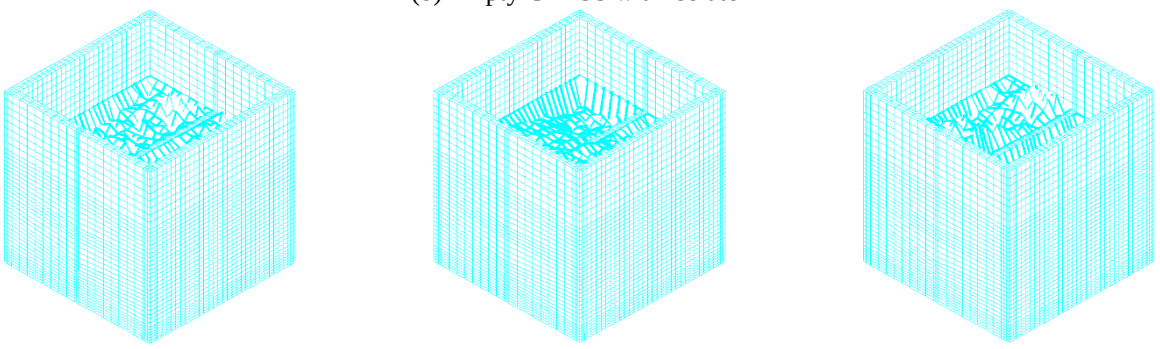

(f_1=0.2456) (f_2=0.3742) (f_3=0.5438)

(c) Liquid filled CRLSS with isolator

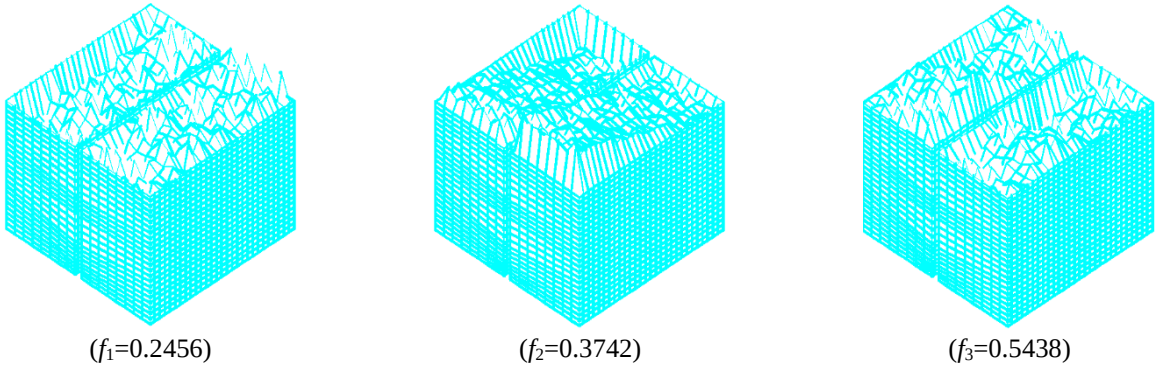

(f_1=0.2456) (f_2=0.3742) (f_3=0.5438)

(d) Liquid

Fig. 6 First three mode shape and frequencies corresponding to 1 baffle with 9 holes

bottom of the isolation layer.

4.1 Case of 1 baffle with 4 holes

The FEM models about the wallboard of a CRLSS of 1 baffle with 4 holes and liquid are shown in Fig. 2. CRLSS is divided into 2 parts in the x direction by 1 baffle. At the same time, the baffle opens 4 holes to connect 2 liquid zones. The height of the baffle is 3.6 m, and the thickness is 0.2 m. To obtain a more accurate response of a CRLSS with

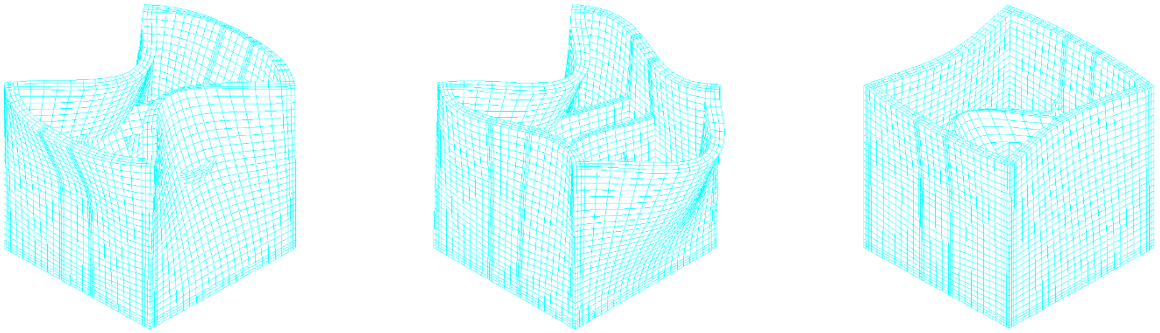

(f_1=26.14) (f_2=26.48) (f_3=27.32)

(a) Empty CRLSS without isolator

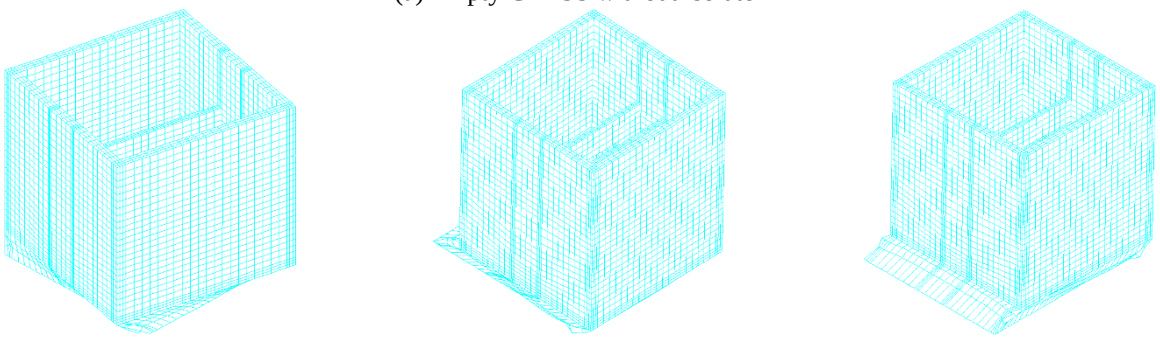

(f_1=2.417) (f_2=2.893) (f_3=2.905)

(b) Empty CRLSS with isolator

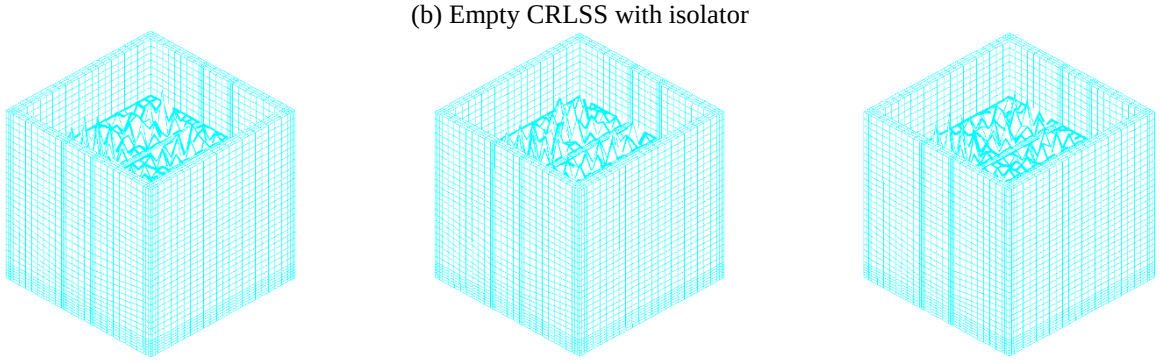

(f_1=0.2818) (f_2=0.4035) (f_3=0.6813)

(c) Liquid filled CRLSS with isolator

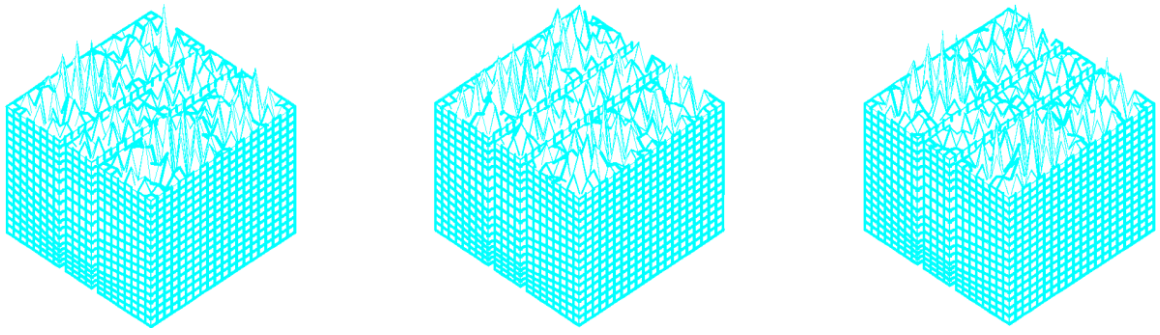

(f_1=0.2818) (f_2=0.4035) (f_3=0.6813)

(d) Liquid

Fig. 6 First three mode shape and frequencies corresponding to 1 baffle with 9 holes

baffles under the various loads, the baffle is divided into three layers in the direction of the thickness.

4.2 Case of 1 baffle with 9 holes

The FEM models about the wallboard of a CRLSS of 1 baffle with 9 holes and liquid are shown in Fig. 3. The CRLSS is divided into 2 parts in the x direction. At the same time, the baffle opens 9 holes to connect 2 zones of liquid. The height of the baffle is 3.6 m, and the thickness is 0.2 m.

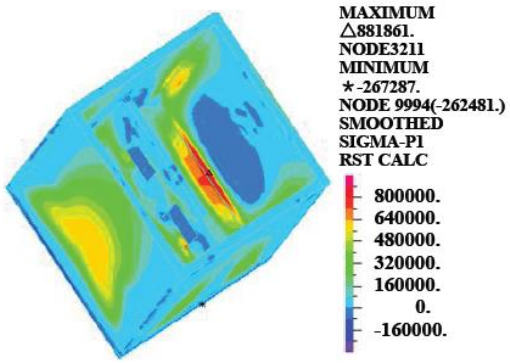

(a) The principal stress distribution nephogram

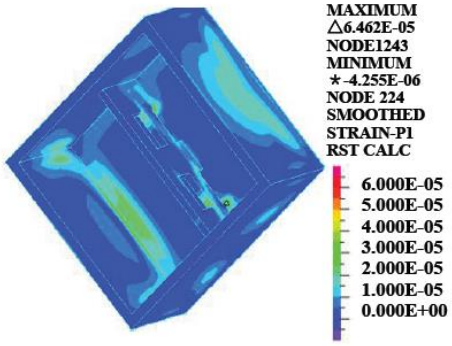

(b) The principal strain distribution nephogram

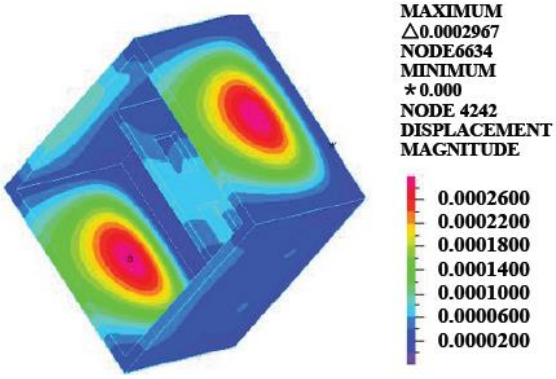

(c) The wallboard displacement distribution nephogram

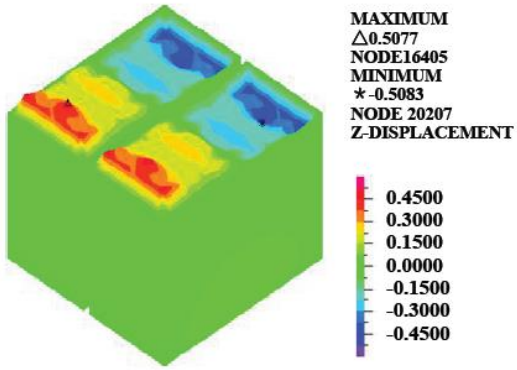

(d) The wave height of the liquid surface distribution nephogram

Fig. 8 Dynamic response of 1 baffle with 4 holes

4.3 Case of 2 baffles with 8 holes

The FEM models about the wallboard of a CRLSS of 2 baffles with 8 holes and liquid are shown in Fig. 4. The CRLSS is divided into 3 parts by 2 baffles in the x direction. At the same time, each baffle opens 4 holes to connect 2 zones of liquid. The heights of both baffles are 3.6 m, and the thicknesses are 0.2 m.

5. Dynamic response of FSI

To study the dynamic response law of a CRLSS under earthquake, the El Centro wave is chosen to carry out the time history dynamic analysis on the interaction system, which was recorded from Imperial Valley earthquake in El-Centro station happened on May 18, 1940. It is a typical near field seismic record. The principal stress, principal strain, displacement, and range of liquid surface fluctuation of the CRLSS with various baffle arrangements are then obtained.

5.1 Modal analysis

The first three order frequencies of the CRLSS with baffle are shown in Figs. 5-7.

5.2 Dynamic response of CRLSS with different baffles and holes

5.2.1 Condition of 1 baffle with 4 holes

The principal stress distribution nephogram of an isolated CRLSS of 1 baffle with 4 holes is shown in Fig. 8(a). The principal strain distribution nephogram of the isolated liquid storage structure of 1 baffle with 4 holes is shown in Fig. 8(b). The wallboard displacement distribution nephogram of an isolated CRLSS of 1 baffle with 4 holes is shown in Fig. 8(c). The wave height of the liquid surface distribution nephogram of an isolated CRLSS of 1 baffle with 4 holes is shown in Fig. 8(d).

According to Fig. 8(a), the maximum principal tensile stress of an isolated CRLSS of 1 baffle with 4 holes is 881.86 kPa, and the maximum principal pressure stress is 267.29 kPa. The maximum principal tensile stress appears at the junction of the board in the y direction and the soleplate of the CRLSS. From Fig. 8(b), the maximum principal strain of the isolated CRLSS of 1 baffle with 4 holes is 6.46×10^{-5}, and it appears at the junction of the baffle and soleplate of the CRLSS. From Fig. 8(c), the maximum displacement of the isolated CRLSS of 1 baffle with 4 holes is 0.297 mm, and it appears in the middle of the board in the y direction of the CRLSS. From Fig. 8(d), the maximum wave height of the isolated CRLSS of 1 baffle with 4 holes is 0.508 m.

5.2.2 Case of 1 baffle with 9 holes

The principal stress distribution nephogram of an isolated CRLSS of 1 baffle with 9 holes is shown in Fig. 9(a). The principal strain distribution nephogram of an isolated CRLSS of 1 baffle with 9 holes is shown in Fig. 9(b). The wallboard displacement distribution nephogram

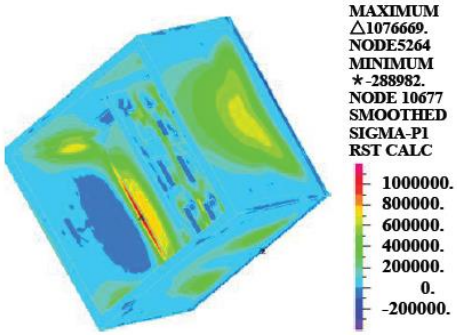

(a) The principal stress distribution nephogram

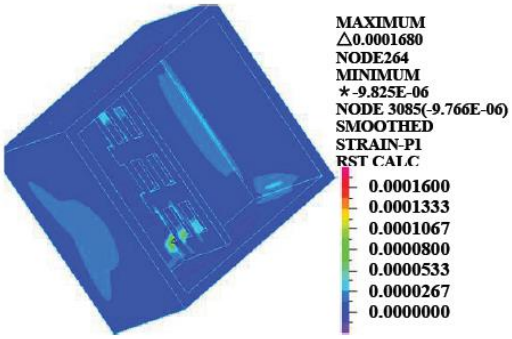

(b) The principal strain distribution nephogram

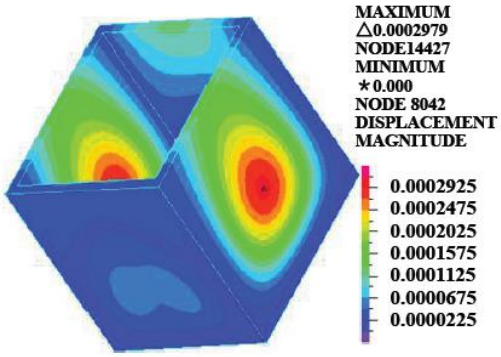

(c) The wallboard displacement distribution nephogram

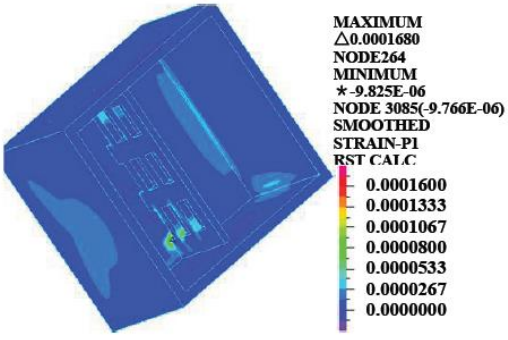

(d) The wave height of the liquid surface distribution nephogram

Fig. 9 Dynamic response of 1 baffle with 9 holes

of an isolated CRLSS of 1 baffle with 9 holes is shown in Fig. 9(c). The wave height of the liquid surface distribution nephogram of the isolated CRLSS of 1 baffle with 9 holes is shown in Fig. 9(d).

According to Fig. 9(a), the maximum principal tensile stress of the isolated CRLSS of 1 baffle with 9 holes is 1076.67 kPa, and the maximum principal pressure stress is 288.98 kPa. The maximum principal tensile stress appears

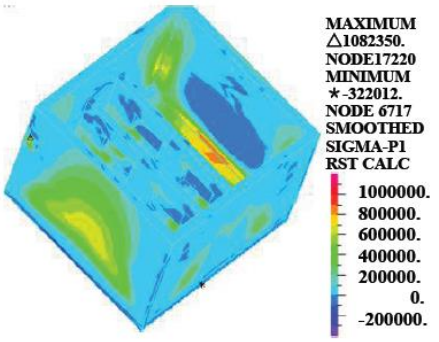

(a) The principal stress distribution nephogram

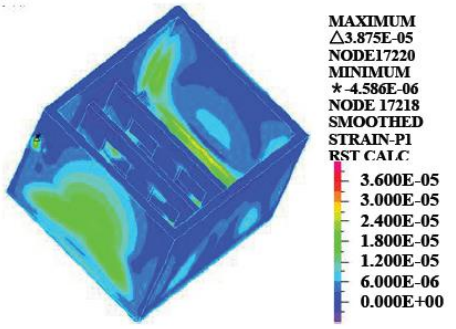

(b) The principal strain distribution nephogram

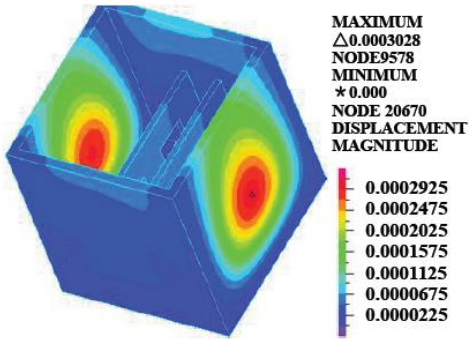

(c) The wallboard displacement distribution nephogram

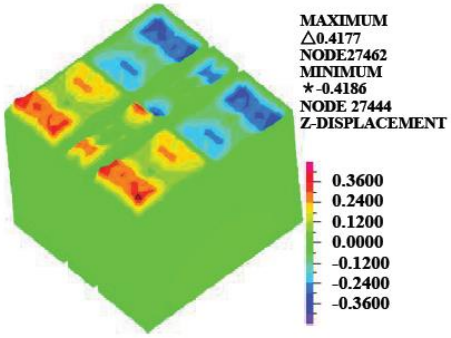

(d) The wave height of the liquid surface distribution nephogram

Fig. 10 Dynamic response of 2 baffles with 8 holes

Table 3 Dynamic responses for the different baffle arrangements

Dynamic responses	1 baffle with 4 holes	1 baffle with 9 holes	2 baffles with 8 holes
Tension stress (MPa)	0.8819	1.0767	1.0824
Compressive stress (MPa)	0.2673	0.2890	0.3320
Strain ($\times 10^{-4}$)	0.6460	1.6860	0.3875
Displacement (mm)	0.2970	0.2980	0.3030
Wave height (m)	0.5080	0.7230	0.4180

at the junction of the wallboard in the *y* direction and soleplate of the CRLSS. From Fig. 9(b), the maximum principal strain of the isolated CRLSS of 1 baffle with 9 holes is 1.686×10^{-4}, and it appears at the junction of the baffle and floor of the CRLSS. From Fig. 9(c), the maximum displacement of the isolated CRLSS of 1 baffle with 9 holes is 0.298 mm, and it appears in the middle of the wallboard in the y direction of the CRLSS. From Fig. 9(d), the maximum wave height of the isolated CRLSS of 1 baffle with 9 holes is 0.723 m.

5.2.3 Case of 2 baffles with 8 holes

The principal stress distribution nephogram of the isolated CRLSS of 2 baffles with 8 holes is shown in Fig. 10(a). The principal strain distribution nephogram of the isolated CRLSS of 2 baffles with 8 holes is shown in Fig. 10(b). The wallboard displacement distribution nephogram of the isolated CRLSS of 2 baffles with 8 holes is shown in Fig. 10(c). The wave height of the liquid surface distribution nephogram of the isolated CRLSS of 2 baffles with 8 holes is shown in Fig. 10(d).

According to Fig. 10(a), the maximum principal tensile stress of the isolated CRLSS of 2 baffles with 8 holes is 1082.35 kPa, and the maximum principal pressure stress is 322.01 kPa. The maximum principal tensile stress appears at the junction of the wallboard in the *y* direction and the wallboard in the *x* direction of the CRLSS. From Fig. 10(b), the maximum principal strain of the isolated CRLSS of 2 baffles with 8 holes is 3.875×10^{-5}, and it appears at the junction of the wallboard in the *y* direction and at the wallboard in the *x* direction of the CRLSS. From Fig. 10(c), the maximum displacement of the isolated CRLSS of 2 baffles with 8 holes is 0.3028 mm, and it appears in the middle of the wallboard in the *y* direction of the CRLSS. From Fig. 10(d), the maximum wave height of the isolated CRLSS of 2 baffles with 8 holes is 0.418 m.

5.3 Result comparison with different baffle arrangements

To provide the reference for the shock-absorbing designs of the baffles of CRLSS, the dynamic responses of the stress, strain and displacement of the structure wallboard are compared with the wave height of liquid sloshing under different baffle arrangements (see Table 3).

As shown in Table 3, the stress, strain, displacement and wave height corresponding to 1 baffle with 4 holes are all less than those of 1 baffle with 9 holes. When adopting 1 baffle arrangement, the wallboard strain and the wave height of liquid sloshing have a great effect if the number of holes is increased. Namely, when the baffle number is certain, the shock-absorbing capacity will decline if there are more holes. When 1 baffle with 4 holes is arranged in parallel with 2 baffles with 8 holes, it is observed that although the corresponding stress and wallboard displacement with holes increase corresponding to the 2 baffles, the wallboard strain and the height of liquid sloshing decrease. Generally, the common failure mode of a CRLSS is leakage of liquid caused by wallboard cracking or excessive wave height caused by liquid sloshing. For a CRLSS with a top plate, the top plate will be destroyed by the impact force produced by an excessive wave of liquid sloshing. For a CRLSS without a top plate, the outflow of liquid from the CRLSS is caused by the excessive wave height of liquid sloshing.

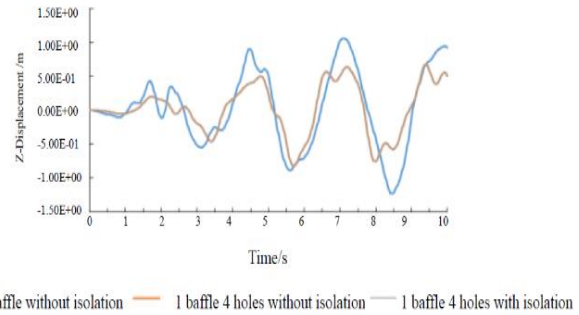

Fig. 11 Contrast curve about the heights of the liquid sloshing

5.4 The influence of isolation on the heights of the liquid sloshing

In order to analyze the control effect of isolation on liquid sloshing height, the curves of the liquid sloshing height about 0 baffle without isolation, 1 baffle 4 holes without isolation, and 1 baffle 4 holes with isolation of CRLSS are shown in Fig. 11.

6. Conclusions

(1) When the baffle number is certain, the greater the number of holes, the greater the stress, strain, wallboard displacement and range of liquid surface fluctuation of the CRLSS. That is, the shock-absorbing capacity will be declined if there are more holes.

(2) The strain and the range of liquid surface fluctuation of a CRLSS with 2 baffles are less than those of 1 baffle. That is, increasing baffles can effectively reduce the wallboard strain and the range of liquid surface fluctuation.

(3) Common failure modes of a CRLSS are wallboard cracking and excessive wave height of liquid sloshing. The dynamic response of the CRLSS itself and the liquid shaking effect can be reduced after setting baffles for the isolated CRLSS. In general, a configuration with fewer holes in the baffles and more baffles in the CRLSS is helpful to prevent the occurrence of the main failure modes of CRLSS, which are wallboard cracking and excessive

sloshing wave height.

Conflict of interests

The authors declare that there is no conflict of interest regarding the publication of this paper.

Acknowledgments

This paper is a part of the National Natural Science Foundation of China (Grant number: 51478212 and 51368039), and the Support Project of Science and Technology in Gansu Province (Grant number: 144GKCA032).

References

Bao, G.W. (2003), Equivalent mechanical model of liquid sloshing in horizontal cylindrical container", *JsShanghai Jiaotong Univ*., **37**(12), 1961-1968.

Bouabidi, A., Driss, Z. and Abid, M.S. (2013), "Vertical baffles height effect on liquid sloshing in an accelerating rectangular tank", *Int. J. Mech. Appl*., **3**(5), 105-116.

Chen, H.J. (2008), *Research of Numerical Method on Railroad Tanker about Solid-Fluid Interaction Problem*, Dalian Jiaotong University, Dalian, China.

Cheng, X.S., Cao, L.L. and Zhu, H.Y. (2015c), "Liquid-solid interaction seismic response of an isolated overground rectangular reinforced-concrete liquid-storage structure", *J. Asian Architect. Build*., **14**(1), 175-180.

Cheng, X.S., Chen, W.J. and Zhu, H.Y. (2015a), "Effects of base isolation on seismic response of concrete rectangular tank", *Elec. J. Geotech. Eng*., **20**(8), 2149-2166.

Cheng, X.S., Zhao, L. and Zhang A.J. (2015b), "FSI resonance response of liquid-storage structures made of rubber-isolated rectangular reinforced concrete", *Elec. J. Geotech. Eng*., **20**(7), 809-1824.

Eswaran, M., Reddy, G.R. and Singh, R.K. (2015), "Effect of higher modes and multi-directional seismic excitations on power plant liquid storage pools", *Earthq. Struct*., **8**(3), 779-799.

Goudarzi, M.A. and Alimohammadi, S. (2010), "Numerical assessment of seismic safety of liquid storage tanks and performance of base isolation system", *Struct. Eng. Mech*., **35**(6), 759-772.

Jadhav, M.B. and Jangid, R.S. (2006), "Response of base-isolated liquid storage tanks to near-fault motions", *Struct. Eng. Mech*., **23**(6), 615-634.

Jia, S.B., Xu, C.X. and Tan, J.K. (2012), "Rectangular container 3D liquid sloshing characteristics study", *Wat. Res. Pow*., **30**(1), 142-144.

Kianoush, M.R. and Ghaemmaghami, A.R. (2011), "The effect of earthquake frequency content on the seismic behavior of concrete rectangular liquid tanks using the finite element method incorporating soil-structure interaction", *Eng. Struct*., **33**(7), 2186-2200.

Li, Q., Ma, X.R. and Wang, T.S. (2011), "Equivalent mechanical model for liquid sloshing in non-axisymmetric tanks", *J. Astro*., **32**(2), 242-249.

Liu, F., Tong, M.B. and Chen, J.P. (2010), "Numerical simulation of three-dimensional liquid sloshing based on SPH method", *J. Nanjing Univ. Aero. Astro*., **42**(1), 122-126.

Livaoglu, R., Cakir, T., Dogangun, A. and Aytekin, M. (2011), "Effects of backfill on seismic behavior of rectangular tanks", *Ocean Eng*., **38**(10), 1161-1173.

Mirzabozorg, H., Hariri-Ardebili, M.A. and Nateghi, A. (2012), "Free surface sloshing effect on dynamic response of rectangular storage tank", *Am. J. Flu. Dyn*., **2**(4), 23-30.

Nayak, S.K. and Biswal, K.C. (2013), "Quantification of nonlinear seismic response of rectangular liquid tank", *Struct. Eng. Mech*., **47**(5), 599-622.

Panchal, V.R. and Soni, D.P. (2014), "Seismic behavior of isolated fluid storage tanks: A-state-of-the-art review", *KSCE J. Civil Eng*., **18**(4), 1097-1104.

Sun, Y., Sun, J.G. and Cui, L.F. (2011), "Floating roof tank numerical simulation analysis under earthquake load", *Sci. Technol. Eng*., **11**(19), 4657-4659.

Virella, J.C., Prato, C.A. and Godoy, L.A. (2008), "Linear and nonlinear 2D finite element analysis of sloshing modes and pressures in rectangular tanks subject to horizontal harmonic motions", *J. Sound Vibr*., **312**(3), 442-460.

Vosoughifar, H.R. and Naderi, M.A. (2014), "Numerical analysis of the base-isolated rectangular storage tanks under bi-directional seismic excitation", *Brit. J. Math. Comput. Sci*., **4**(21), 3054.

Wilson, E.L. (2002), *Three Dimensional Static and Dynamic Analysis of Structure*, 3rd Edition, Computers and Structures, Inc.

Zhao, L.H., Li, T.C. and Niu, Z.W. (2006), "Rigid container flow numerical simulation of nonlinear swings", *J. Hehai Univ*., **34**(4), 401-405.

CC